Nanoscale

CrossMark
click for updates

Hybrid van der Waals heterostructures of zero-dimensional and two-dimensional materials†

Zhikun Zheng,*[a,b] Xianghui Zhang,[a] Christof Neumann,[a] Daniel Emmrich,[a] Andreas Winter,[c] Henning Vieker,‡[a] Wei Liu,[d] Marga Lensen,[e] Armin Gölzhäuser[a] and Andrey Turchanin*[c]

van der Waals heterostructures meet other low-dimensional materials. Stacking of about 1 nm thick nanosheets with out-of-plane anchor groups functionalized with fullerenes integrates this zero-dimensional material into layered heterostructures with a well-defined chemical composition and without degrading the mechanical properties. The developed modular and highly applicable approach enables the incorporation of other low-dimensional materials, *e.g.* nanoparticles or nanotubes, into heterostructures significantly extending the possible building blocks.

Molecular assembly of materials with precise control over their chemical composition, thickness and structure has been in the focus of physical, chemical and materials science research already for many years.[1–9] This interest is motivated by engineering materials with controlled functionalities on demand. To this end, various techniques have been developed. Typical examples are Langmuir–Blodgett (LB) technique, layer-by-layer (LbL) assembly, and self-assembled monolayers (SAMs). They have been widely used to assemble zero- and one-dimensional (0D and 1D) materials such as small molecules, nanoparticles, biomolecules, polyelectrolytes and nanotubes/-wires.[1–8] With the demonstration of free-standing atomically or single-molecularly thick sheets,[10–12] stacking them vertically in a chosen way serves as a new technique to create designed artificial materials, the so-called van der Waals (vdW) heterostructures.[9,13,14] Combination of these 2D sheets including graphene, hexagonal boron nitride or metal chalcogenides has led to mechanically stable heterostructures with high potential for applications in sensors and flexible electronics.[9,15] Recent research efforts have also been focused on the development of various covalent and non-covalent functionalization approaches to combine 2D sheets with 0D and 1D materials.[16–20] However, it remains a major challenge to assemble stable stacks of 0D/1D materials with 2D sheets without degrading the mechanical properties of the pristine sheets. Non-covalent interactions, such as van der Waals interactions and π–π stacking, are not strong enough to stably immobilize 0D/1D materials on 2D sheets. Thus the adhered materials can be easily removed by solvent rinsing or even with time and by environmental moisture.[16,19,20] On the other hand, strong covalent interactions require a change in the integral structure of 2D sheets, which degrade their initial mechanical properties.

In this work, we present a modular and broadly applicable route to create hybrid vdW heterostructures made of individual ~1 nm thick single molecular sheets, Janus nanomembranes (JNMs),[13,21] which have well-defined anchor groups on their opposite sides, see Fig. 1, and other low-dimensional materials. JNMs are generated *via* electron irradiation of 4′-nitro-1,1′-biphenyl-4-thiol (NBPT) SAMs resulting in their crosslinking *via* formation of lateral covalent bonds and simultaneous conversion of the terminal nitro groups into amino groups[22] and the subsequent release from the original substrates *via* the poly(methyl methacrylate) (PMMA) assisted transfer process.[23,24] The upper side of the JNM has amino groups (N-side) and the lower side has sulfur species (S-side), see Fig. 1c; both sides can be independently and chemically functionalized.[21] Using chemical functionalization of JNMs with the desired building blocks on their one or both faces and subsequent stacking, hybrid vdW heterostructures can be assembled. In our proof-of-concept experiments, we utilize 0D carbon – fullerene C_{60} – as a functional nanomaterial and covalently bind to the amino groups of JNMs; we also demonstrate functionalization of the S-side with Au nanoparticles (NPs), see Fig. 1d. We fabricate heterostructure stacks of the C_{60}–JNM hybrid and characterize their structural, chemical and mechanical properties by optical microscopy, helium ion microscopy

[a]*Faculty of Physics, University of Bielefeld, 33615 Bielefeld, Germany*
[b]*Department of Chemistry and Food Chemistry, TU Dresden, 01069 Dresden, Germany. E-mail: zhikun.zheng@tu-dresden.de*
[c]*Institute of Physical Chemistry, Friedrich Schiller University Jena, 07743 Jena, Germany. E-mail: andrey.turchanin@uni-jena.de*
[d]*Physical Chemistry and Center for Advancing Electronics Dresden, TU Dresden, 01069 Dresden, Germany*
[e]*Institute of Chemistry, Technische Universität Berlin, 10623 Berlin, Germany*
†Electronic supplementary information (ESI) available. See DOI: 10.1039/c5nr03475b
‡Current address: CNM Technologies, 33602 Bielefeld, Germany.
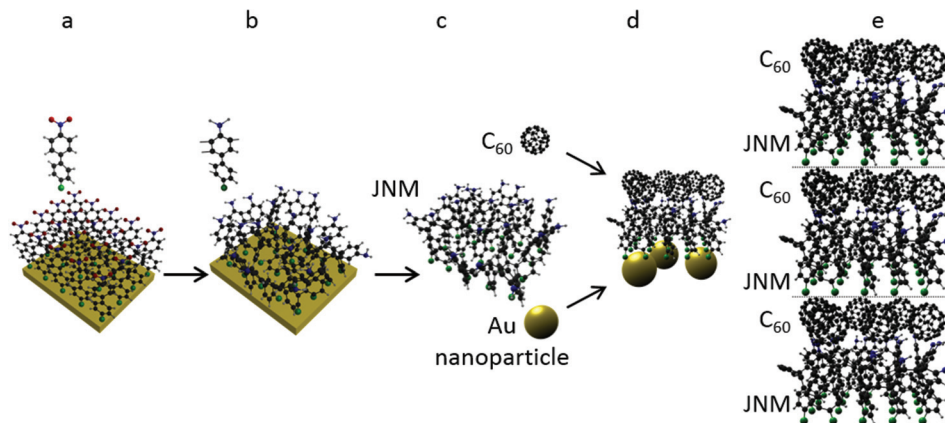
Fig. 1 Schematic representation of the heterostructure assembly. (a) Formation of a NBPT SAM on a gold substrate. (b) Electron irradiation induced crosslinking and reduction of the terminal nitro groups into amino groups. (c) Formation of a free-standing JNM with the terminal N- and S-faces. (d) Functionalization of the N- and S-faces with C_{60} and AuNP, respectively. (e) Assembly of a $(C_{60}-JNM)_n$ (here $n = 3$) hybrid heterostructure by mechanical stacking. Color code for atoms: black – carbon, grey – hydrogen, blue – nitrogen, green – sulfur, and red – oxygen.

(HIM), X-ray photoelectron spectroscopy (XPS) and mechanical bulging tests. To make the S-side of JNMs accessible for post-modification under various experimental conditions, a universal flip-over procedure for JNMs was developed.

To assemble C_{60}–JNM heterostructures, we synthesized JNMs on gold substrates (JNM/Au), immobilized C_{60} onto the N-side of the JNMs, and stacked the C_{60}–JNM hybrids on top of each other (see ESI† for details). The successful immobilization of C_{60} onto JNM/Au was confirmed by XPS. Fig. 2a shows the XP spectra of a JNM/Au. The C1s signal consists of several peaks with binding energies (BEs) at 284.2 eV and 285.3 eV, which are due to the aromatic carbon and the C–S/C–N bonds, respectively; and the aromatic shake-up satellites at 287–290 eV.[24] The N1s signal at 399.3 eV is characteristic for amino groups. The S2p signal shows the presence of two sulfur species with the $S2p_{3/2}$ BEs at 162.0 and 163.2 eV, which are due to thiolates and sulfides/disulfides formed upon irradiation,[25] respectively. The effective thickness of a JNM calculated from the attenuation of the $Au4f_{7/2}$ signal is about 1.1 nm.[26] In Fig. 2b, the XP spectra of a JNM with C_{60} grafted to the amino groups are presented.[27] The successful grafting is confirmed by the corresponding changes of the respective XP signals. The total intensity of the C1s signal increases by ~30% and a new N1s peak at ~400.3 eV appears due to the formation of C–N bonds.[27–29] The intensity ratio between this peak and the total N1s intensity is ~30%, which indicates the percentage of amino groups on forming chemical bonds with C_{60}. Intensity of the S2p signal decreases showing an increase of the hybrid thickness (see Table S1† for thickness change).

To demonstrate that C_{60}–JNMs can be released from their original substrate and further used for fabrication of the heterostructures, we tested their transfer onto 285 nm SiO_2/Si substrates by the PMMA assisted process.[24] These substrates were chosen as they enable the observation of JNMs by optical interference (see Fig. S1a†).[14] Fig. 2c shows XP spectra of the transferred C_{60}–JNM. The characteristics of the XP signals are
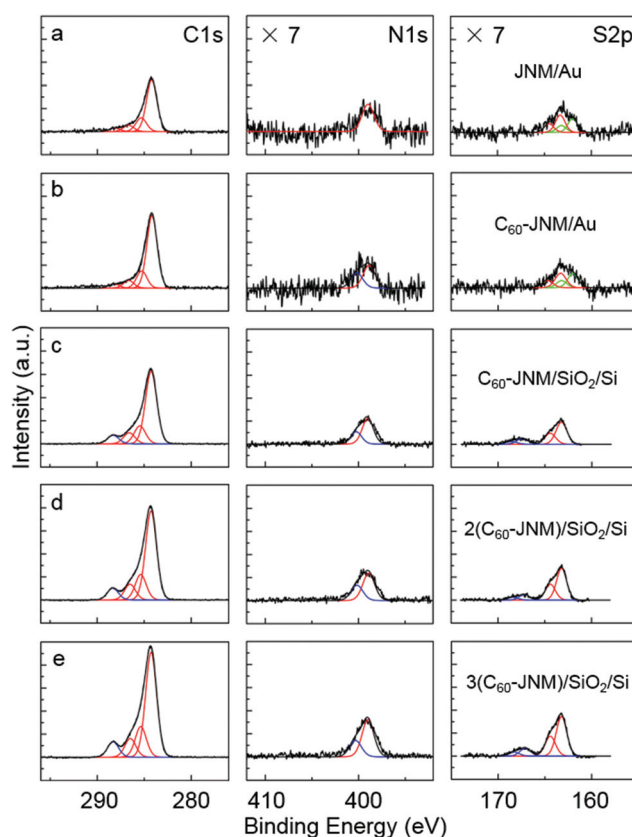
Fig. 2 XPS characterization. (a) JNM on the original gold substrate. (b) C_{60}–JNM on the original gold substrate. C_{60}–JNM monolayer/multilayer after transfer onto 285 nm SiO_2/Si (monolayer (c), bilayer (d) and trilayer (e)). Intensities of the S2p and N1s spectra were multiplied by 7.

similar to those of the pristine C_{60}–JNM/Au. A slight increase of the C1s peak at ~288.3 eV is observed, which is most likely due to the presence of some PMMA residuals after the transfer.[30] The $S2p_{3/2}$ signal at 162.0 eV disappears and the inten-

sity of the S2p$_{3/2}$ signal at 163.2 eV increases significantly due to the transformation of thiolates into sulfides/disulfides or into unbound thiols during the transfer process.[21] A new doublet appears with S2p$_{3/2}$ at 167.2 eV caused by the oxidation of thiolates/sulfides/disulfides into the sulfonic group.[31] Note that the sulfonic group is negatively charged in water, which can be used for the functionalization of the S-side of JNMs by electrostatic interactions.

For the fabrication of cm^2-sized patterned C$_{60}$–JNM heterostructures on 285 nm SiO$_2$/Si, a simple method was applied. C$_{60}$–JNM sheets on Au/mica substrates were cut with scissors into rectangular stripes of ~0.5 cm width and then the sheets were transferred onto the Si-wafer by putting them on top of each other in different orientations. This procedure leads to the formation of regions with either no, one, two or three sheets (Fig. S1a†). Note that the uniform contrast within the areas with varying numbers of C$_{60}$–JNM sheets reflects their homogeneous thickness.

As only the electron irradiated areas of NBPT SAMs are converted into JNMs and there is no lateral crosslinking between molecules in the non-irradiated areas, it is possible by selective electron irradiation to pattern JNMs, functionalize them with C$_{60}$ and then transfer the patterned C$_{60}$–JNM onto a new substrate (Fig. S1b†). Such a procedure makes it possible to produce the JNM-based hybrids in any shape without additional resist materials either by using electron irradiation through stencil masks, as in this experiment, or by standard electron beam lithography.

The assembled heterostructure stacks were characterized by XPS. We found no significant changes in the shapes of C1s, S2p and N1s signals for the bi-layer and the tri-layer of C$_{60}$–JNM (Fig. 2d and e), which indicates that each layer has a similar chemical composition. The obtained effective thickness of the bi-layer and tri-layer stacks is ~3.7 nm and ~5.4 nm, respectively, which confirms further homogeneous contributions of each layer to the total structure. This homogeneity benefits from the high reproducibility by functionalization of mechanically stable JNMs, which is difficult to achieve employing the layer-by-layer growth on conventional SAMs.[32–34]

To quantitatively characterize the mechanical properties of individual C$_{60}$–JNMs and their heterostructures, they were studied by mechanical bulge tests. To this end, the sheets were transferred onto a silicon substrate with an array of square shaped orifices. Fig. 3a shows a helium ion microscopy (HIM) image of a C$_{60}$–JNM hybrid. An orifice with the spanned C$_{60}$–JNM is observed (marked "freestanding"), which indicates that the hybrid can support its own weight and preserve its mechanical integrity. Apart from the large homogeneous area, some wrinkles or ruptures (Fig. 3b and c) are observed, which are typical for mechanically robust nanosheets.[10] Fig. 3d shows a homogeneous freestanding JNM/(C$_{60}$–JNM)$_3$ heterostructure spanning over an orifice with dimensions of 40 × 44 μm^2. The heterostructure in Fig. 3e shows some wrinkles, which increase the imaging contrast and help to identify the freestanding membrane by HIM. Note that only the homogeneous structures as in Fig. 3d were employed for bulge tests with an atomic force microscope (AFM). To ensure that the interaction between a (C$_{60}$–JNM)$_n$ and an AFM tip is the same as that for an individual JNM, a JNM was placed on top of the respective heterostructures forming the JNM/(C$_{60}$–JNM)$_n$ stacks. The testing was performed by adjusting an AFM tip to the nano-
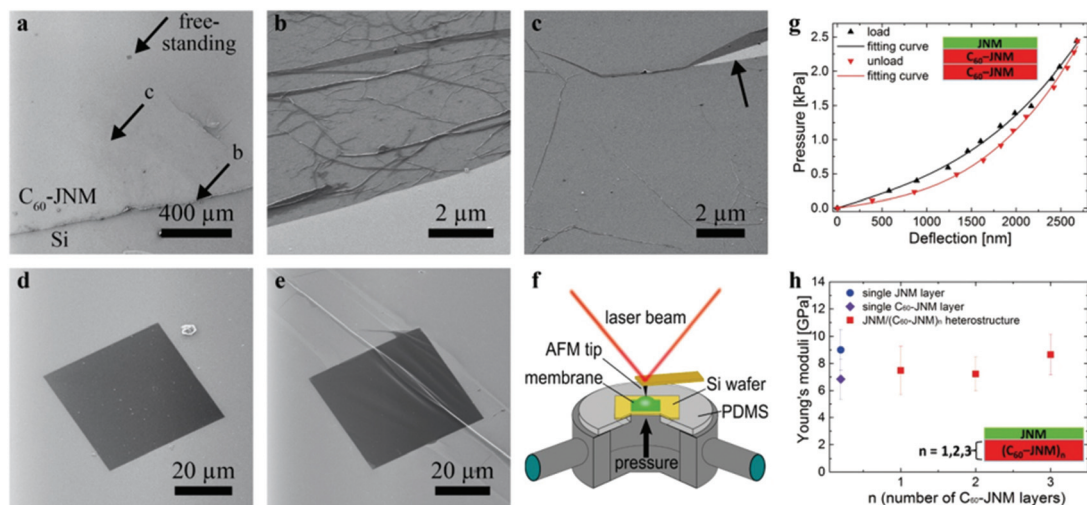
Fig. 3 Helium ion microscopy (HIM) imaging of C$_{60}$–JNM heterostructures and their mechanical properties. (a) HIM image of a C$_{60}$–JNM on a Si substrate with orifices. An orifice with dimensions 40 × 44 μm^2 is marked here as "free-standing". (b) Magnified HIM image of the C$_{60}$–JNM boundary; the corresponding place is marked in (a) with an arrow. (c) Magnified HIM image of the central part of the C$_{60}$–JNM; the corresponding place is marked in (a) with an arrow. In (d) and (e) HIM images of an JNM–(C$_{60}$–JNM)$_3$ heterostructure spanning a Si window are shown. In (d) the nanomembrane is homogeneous whereas in (e) a fold can be recognized. (f) A schematic diagram of the bulge test set-up. (g) Typical pressure-deflection curves for a JNM–(C$_{60}$–JNM)$_2$ heterostructure. (h) Young's moduli of JNM, C$_{60}$–JNM and JNM–(C$_{60}$–JNM)$_n$ (n = 1, 2, and 3).

membrane center,[35,36] as schematically shown in Fig. 3f. Different N_2 pressures are applied beneath the membrane, and its corresponding deflection is then recorded by AFM. Fig. 3g shows a typical pressure-deflection curve for a JNM/(C_{60}–JNM)$_2$ heterostructure (see Fig. S2† for JNM, C_{60}–JNM and JNM/(C_{60}–JNM)$_n$, n = 1 and 3). By fitting multiple curves to a pressure-deflection equation for rectangular/square membranes,[35,36] Young's modulus (E_{Young}) can be extracted (Fig. 3h and Table S1†). First, we compare the mechanical properties of pristine JNM with C_{60}–JNM. To this end, the in-plane elastic modulus (E_{2d}) has to be considered.[37–39] It is equal to E_{Young} multiplied by the thickness of the sheet. The obtained E_{2d} values for JNM (9.9 ± 1.7 N m^{-1}) and C_{60}–JNM (11.6 ± 1.7 N m^{-1}) are of the same magnitude, which shows that the mechanical robustness of a JNM is not diminished upon its covalent functionalization. Next, we compare the mechanical properties of multilayered stacks considering the respective E_{Young} values.[37] E_{Young} for JNM/(C_{60}–JNM)$_1$, JNM/(C_{60}–JNM)$_2$ and JNM/(C_{60}–JNM)$_3$ are 7.5 ± 1.8 GPa, 7.2 ± 1.3 GPa and 8.7 ± 1.5 GPa, respectively (Fig. 3h). It can be clearly seen that within the measurement accuracy the Young's moduli of the JNM/(C_{60}–JNM)$_n$ (n = 1, 2 and 3) heterostructures have similar values demonstrating that the mechanical properties are not degraded upon the assembly of the hybrid JNMs into stacks.

To show that for the assembly of hybrid heterostructures the S-side of JNMs can also be employed, we studied its functionalization with Au NPs (Fig. 1c and Fig. 4). Negatively charged Au NPs with sizes of ~55 and 16 nm were used to this end. As the S-side of a JNM due to the presence of sulfonic groups is also negatively charged, a positively charged adhesive polyelectrolyte layer of poly(diallyldimethylammonium chloride) was added to immobilize the negatively charged Au NPs. We employed scanning transmission ion microscopy (STIM) to image the hybrid nanomembranes suspending hexagonal grids (~25 μm) with the functionalized S-side oriented upwards. From statistical analysis we estimate the average coverage of the 55 and 16 nm-sized Au NPs on JNMs to be ~15% and ~50%, respectively, showing that the coverage correlates with the NP size. As a wide variety of materials can be immobilized by electrostatic interactions,[2] this strategy provides a flexible route to incorporate different materials into JNM-based hybrids. The modification of the S-side of JNMs with the above-described method needs PMMA as a protection layer, which restricts the modification to conditions compatible with this layer. In case such a layer cannot be employed, the JNM can also be flipped over and transferred onto a new solid substrate where the originally bottom S-side becomes the terminal one (Fig. S3–5†).

Conclusions

In summary, we have presented a modular and highly applicable approach for the assembly of cm^2-sized vdW hybrid heterostructures. This approach is based on the utilization of ~1 nm thick bifacial and mechanically stable JNMs, their chemical functionalization and subsequent stacking into layered heterostructures. In the present study the heterostructures of JNMs with C_{60} and gold nanoparticles were investigated. The possibility of bifacial chemical functionalization of
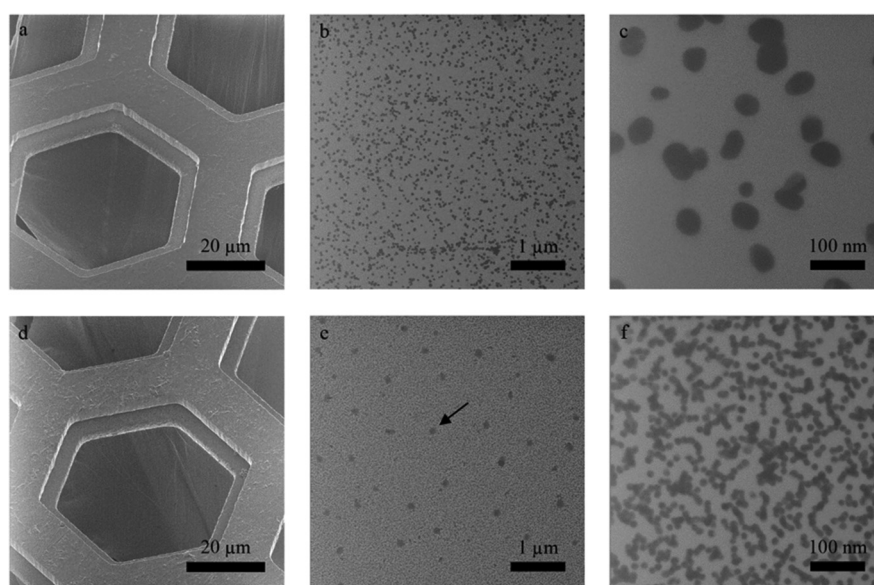
Fig. 4 JNMs functionalized with Au nanoparticles on the S-face. Helium ion microscope images acquired in the secondary electron (SE) mode and scanning transmission ion mode (STIM). (a) SE image of JNMs functionalized with 55 nm Au nanoparticles and transferred onto a grid. (b) and (c) STIM images show that the nanoparticles are uniformly distributed with an average coverage of ~15%. (d) SE image of JNMs functionalized with 16 nm Au nanoparticles and transferred onto a grid. (e) and (f) STIM images showing that the nanoparticles are uniformly distributed with a coverage of ~50%. Dark areas (see the arrow in (e)) are residues from sample preparation.

JNMs paves the way to hybrid vdW heterostructures with a variety of other 0D and 1D materials.

Acknowledgements

Notes and references

1 K. B. Blodgett, *J. Am. Chem. Soc.*, 1934, **56**, 495.

2 G. Decher, *Science*, 1997, **277**, 1232.

3 K. Ariga, J. P. Hill and Q. Ji, *Phys. Chem. Chem. Phys.*, 2007, **9**, 2319.

4 S. Srivastava and N. A. Kotov, *Acc. Chem. Res.*, 2008, **41**, 1831.

5 Z. Tang, Y. L. Wang, P. Podsiadlo and N. A. Kotov, *Adv. Mater.*, 2006, **18**, 3203.

6 J. Sagiv, *J. Am. Chem. Soc.*, 1980, **102**, 92.

7 J. C. Love, L. A. Estroff, J. K. Kriebel, R. G. Nuzzo and G. M. Whitesides, *Chem. Rev.*, 2005, **105**, 1103.

8 A. Ulman, *Introduction to Ultrathin Organic Films*, Academic, San Diego, CA, 1991.

9 A. K. Geim and I. V. Grigorieva, *Nature*, 2013, **499**, 419.

10 K. S. Novoselov, D. Jiang, F. Schedin, T. J. Booth, V. V. Khotkevich, S. V. Morozov and A. K. Geim, *Proc. Natl. Acad. Sci. U. S. A.*, 2005, **102**, 10451.

11 J. Sakamoto, J. van Heijst, O. Lukin and A. D. Schluter, *Angew. Chem., Int. Ed.*, 2009, **48**, 1030.

12 W. Eck, A. Küller, M. Grunze, B. Völkel and A. Gölzhäuser, *Adv. Mater.*, 2005, **17**, 2583.

13 (a) M. Woszczyna, A. Winter, M. Grothe, A. Willunat, S. Wundrack, R. Stosch, T. Weimann, F. Ahlers and A. Turchanin, *Adv. Mater.*, 2014, **26**, 4831; (b) C. T. Nottbohm, A. Turchanin, A. Beyer, R. Stosch and A. Gölzhäuser, *Small*, 2011, **7**, 874.

14 (a) H. Yin, S. Zhao, K. Zhao, A. Muqsit, H. Tang, L. Chang, H. Zhao, Y. Gao and Z. Tang, *Nat. Commun.*, 2015, **6**, 6430; (b) H. Tang, J. Wang, H. Yin, H. Zhao, D. Wang and Z. Tang, *Adv. Mater.*, 2015, **27**, 1117; (c) H. Yin, S. Zhao, J. Wan, H. Tang, L. Chang, L. He, H. Zhao, Y. Gao and Z. Tang, *Adv. Mater.*, 2013, **25**, 6270.

15 T. Georgiou, R. Jalil, B. D. Belle, L. Britnell, R. V. Gorbachev, S. V. Morozov, Y.-J. Kim, A. Gholinia, S. J. Haigh, O. Makarovsky, L. Eaves, L. A. Ponomarenko, A. K. Geim, K. S. Novoselov and A. Mishchenko, *Nat. Nanotechnol.*, 2013, **8**, 100.

16 V. Georgakilas, M. Otyepka, A. B. Bourlinos, V. Chandra, N. Kim, K. C. Kemp, P. Hobza, R. Zboril and K. S. Kim, *Chem. Rev.*, 2012, **112**, 6156.

17 D. Voiry, A. Goswami, R. Kappera, C. C. C. Silva, D. Kaplan, T. Fujita, M. Chen, T. Asefa and M. Chhowalla, *Nat. Chem.*, 2015, **7**, 45.

18 S. Jiang, S. Butler, E. Bianco, O. D. Restrepo, W. Windl and J. E. Goldberger, *Nat. Commun.*, 2014, **5**, 1.

19 H. Y. Mao, Y. H. Lu, J. D. Lin, S. Zhong, A. T. S. Wee and W. Chen, *Prog. Surf. Sci.*, 2013, **88**, 132.

20 J. Du, S. Pei, L. Ma and H.-M. Cheng, *Adv. Mater.*, 2014, **26**, 1958.

21 Z. Zheng, C. T. Nottbohm, A. Turchanin, H. Muzik, A. Beyer, M. Heilemann, M. Sauer and A. Gölzhäuser, *Angew. Chem., Int. Ed.*, 2010, **49**, 8493.

22 W. Eck, V. Stadler, W. Geyer, M. Zharnikov, A. Gölzhäuser and M. Grunze, *Adv. Mater.*, 2000, **12**, 805.

23 A. Turchanin and A. Gölzhäuser, *Prog. Surf. Sci.*, 2012, **87**, 108.

24 A. Turchanin, A. Beyer, C. T. Nottbohm, X. Zhang, R. Stosch, A. S. Sologubenko, J. Mayer, P. Hinze, T. Weimann and A. Gölzhäuser, *Adv. Mater.*, 2009, **21**, 1233.

25 A. Turchanin, D. Käfer, M. El-Desawy, C. Wöll, G. Witte and A. Gölzhäuser, *Langmuir*, 2009, **25**, 7342.

26 M. Schnietz, A. Turchanin, C. T. Nottbohm, A. Beyer, H. H. Solak, P. Hinze, T. Weimann and A. Gölzhäuser, *Small*, 2009, **5**, 2651.

27 P. J. Moriarty, *Surf. Sci. Rep.*, 2010, **65**, 175.

28 K. M. Chen, W. B. Caldwell and C. A. Mirkin, *J. Am. Chem. Soc.*, 1993, **115**, 1193.

29 W. B. Caldwell, K. Chen, C. A. Mirkin and S. J. Babinec, *Langmuir*, 1993, **9**, 1945.

30 A. Pirkle, J. Chan, A. Venugopal, D. Hinojos, C. W. Magnuson, S. McDonnell, L. Colombo, E. M. Vogel, R. S. Ruoff and R. M. Wallace, *Appl. Phys. Lett.*, 2011, **99**, 122108.

31 A. P. Terzyk, *Colloids Surf., A*, 2001, **177**, 23.

32 S. Heid, F. Effenberger, K. Bierbaum and M. Grunze, *Langmuir*, 1996, **12**, 2118.

33 N. Tillman, A. Ulman and T. L. Penner, *Langmuir*, 1989, **5**, 101.

34 H. Sugimura, H. Yonezawa, S. Asai, Q. W. Sun, T. Ichii, K. H. Lee, K. Murase, K. Noda and K. Matsushige, *Colloids Surf., A*, 2008, **321**, 249.

35 X. H. Zhang, A. Beyer and A. Gölzhäuser, *Beilstein J. Nanotechnol.*, 2011, **2**, 826.

36 X. H. Zhang, C. Neumann, P. Angelova, A. Beyer and A. Gölzhäuser, *Langmuir*, 2014, **30**, 8221.

37 C. Lee, X. Wie, J. W. Kysar and J. Hone, *Science*, 2008, **521**, 385.

38 Z. Zheng, C. S. Ruiz-Vargas, T. Bauer, A. Rossi, P. Payamyar, F. Schiffmann, J. VandeVondele, A. Stemmer, J. Sakamoto and A. D. Schlüter, *Macromol. Rapid Commun.*, 2013, **34**, 1670.

39 Z. Zheng, L. Opilik, F. Schiffmann, W. Liu, G. Bergamini, P. Ceroni, L. Lee, A. Schütz, J. Sakamoto, R. Zenobi, J. VandeVondele and A. D. Schlüter, *J. Am. Chem. Soc.*, 2014, **136**, 6103.